ACS APPLIED MATERIALS & INTERFACES

Research Article

www.acsami.org

Carbon/MnO_2 Double-Walled Nanotube Arrays with Fast Ion and Electron Transmission for High-Performance Supercapacitors

Qi Li, Xue-Feng Lu, Han Xu, Ye-Xiang Tong,* and Gao-Ren Li*

MOE Laboratory of Bioinorganic and Synthetic Chemistry, KLGHEI of Environment and Energy Chemistry, School of Chemistry and Chemical Engineering, Sun Yat-sen University, Guangzhou, 510275 Guangdong, China

Supporting Information

ABSTRACT: The novel carbon (C)/MnO_2 double-walled nanotube arrays (DNTAs) are designed and fabricated via template-assisted electrodeposition. The unique DNTA architectures of C/MnO_2 composites with high weight fraction of MnO_2 allow high electrode utilization ratio and facilitate electron and ion transmission. In the half-cell test, the hybrid C/MnO_2 DNTAs as electrodes show a large specific capacitance (C_{sp}) of 793 F/g at the scan rate of 5 mV/s, high energy/power densities, and much enhanced long-term cycle stability. After 5,000 cycles, the C_{sp} retention of C/MnO_2 DNTAs keeps ~97%, which is much larger than 69% of the MnO_2 nanotube arrays (NTAs). The symmetrical supercapacitors (SSCs) composed of C/MnO_2 DNTAs also show the predominant performance, such as large C_{sp} of 161 F/g and high energy density of ~35 Wh/kg, indicating that the C/MnO_2 DNTAs is a potential electrode for supercapacitors. The high order pore passages, double-walled structures, hollow structures, and high conductivity are responsible for the superior performance of C/MnO_2 DNTAs. Such hybrid C/MnO_2 DNTAs may bring new opportunities for the development of supercapacitors with superior performance.

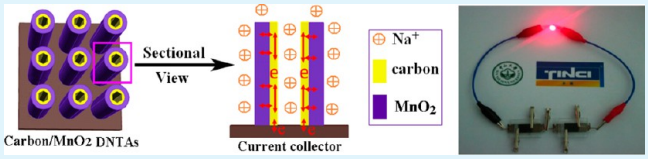

KEYWORDS: *electrodeposition, hybrid material, nanotube array, supercapacitor*

INTRODUCTION

Recently, the energy storage and conversion have attracted wide interest because of the growing demands for energy and increasing concerns with air pollution. Among various energy storage systems, supercapacitors (SCs) have been considered as excellent potential candidates for energy storage because of their higher power density and longer cycle stability than batteries and greater energy density than the conventional electrical double layer capacitors.[1−3] Up to now, the carbonaceous materials,[4,5] metal oxides or hydroxides,[6,7] and conducting polymers[8] as major types of electrode materials have been widely reported for SCs: Carbonaceous materials have long cycle stability and high power density, nevertheless, the low energy density greatly limits their application.[9] By contrast, the conducting polymers, metal oxides, and metal hydroxides enable high energy density, but they are usually kinetically unfavorable.[10,11] Recently, it has inspired attempts to develop novel hybrid electrodes via the coupling of various materials for SCs because of the inherent limitations of above single material.[12−22]

Among the various supercapacitive materials, MnO_2 has been widely thought to be one of the most promising materials for SCs because of its low cost, high abundance, and large theoretical specific capacitance (C_{sp}) and being environmentally-friendly. However, MnO_2 owns the poor conductivity (10^{-5}−10^{-6} S/cm) that limits rate capability for high power performance and still remains a major challenge, thus preventing its wide energy storage applications.[23] To effectively use MnO_2, various MnO_2/conductive matrix hybrid materials, such as MnO_2/Zn_2SnO_4,[24] MnO_2/Au,[25,26] MnO_2/SnO_2,[27] MnO_2/conducting polymers,[28] and carbon (C)/MnO_2,[29] were widely studied. Among them, the C/MnO_2 hybrid materials showed a great potential for the next generation SCs because carbon is light and has high conductivity and good capacitive property.[30,31] At present, in the above various cases, MnO_2 is low weight ratio in hybrid electrodes, and in general it has remarkable cycling and rate performance; however, the power and energy densities are often reduced.[30,32−34] To date, as before it remains a challenge to develop the orderly MnO_2-carbon hybrid electrodes with high weight fraction of MnO_2 and large specific surface area for high energy and power densities demand such as electric vehicles.

Based on the above consideration, here we designed novel C/MnO_2 double-walled nanotube arrays (DNTAs) with high weight fraction of MnO_2 for SCs. The aligned DNTAs show high orderly pore structures. The design of such C/MnO_2 DNTAs shows the following aims: (*i*) As the high electrical conductivity of carbon layers, the fast charge storage and delivery can be realized on carbon layers, and this will help to overcome the limited electric conductivity of MnO_2. In addition, the carbon layers are thin and light, so the weight fraction of MnO_2 in electrodes will be obviously enhanced (~98.94 wt %), and high energy and power densities will be easily achieved. (*ii*) The C/MnO_2 DNTAs will relax ion transport because of the short ion diffusion paths and provide reversible, fast faradic reactions. (*iii*) The DNTAs will improve

Received: November 21, 2013
Accepted: February 6, 2014
Published: February 6, 2014

dx.doi.org/10.1021/am405271q | ACS Appl. Mater. Interfaces 2014, 6, 2726−2733

the utilization rates of electrode materials because of the special double-walled nanotube arrays. (*iv*) The C/MnO_2 DNTAs will let each nanotube can available take part in electrochemical reactions because of excellent electrical contact with current collectors. The results in this study prove that the fabricated C/MnO_2 DNTAs exhibit high C_{sp}, superior rate capability, and great long-term cycle life, and are potential electrode materials for SCs with high performance.

EXPERIMENTAL SECTION

Synthesis of ZnO/C NRAs. ZnO nanorod arrays (ZnO NRAs) were electrodeposited on a Ti substrate in 0.01 M $Zn(NO_3)_2$ + 0.05 M NH_4Cl solution via galvanostatic electrodeposition at a current density of 0.5 mA cm^{-2} for 90 min at 70 °C. Then the fabricated ZnO NRAs (1.0 cm × 1.0 cm) were immersed into a 1.0 M glucose solution for 120 min and dried at 60 °C to yield the glucose modified ZnO nanorods. Finally, the heat treatment process of glucose was carried out at 200 °C for 60 min and then at 400 °C for 120 min under argon for gradual glucose carbonization to yield the carbon-coated ZnO nanorods arrays (ZnO/C NRAs).

Synthesis of C/MnO_2 DNTAs and MnO_2 NTAs. MnO_2 was anodically electrodeposited on the surfaces of ZnO/C NRAs and ZnO NRAs to form ZnO/C/MnO_2 hybrid NRAs and ZnO/MnO_2 hybrid NRAs, respectively, in solution of 0.01 M $Mn(CH_3COO)_2$ + 0.05 M H_3BO_3 + 0.05 M CH_3COONH_4 by galvanostatic electrodeposition at 0.1 mA cm^{-2} at 70 °C for 30 min. The C/MnO_2 double-walled nanotube arrays (DNTAs) and MnO_2 nanotube arrays (NTAs) were synthesized via dissolving ZnO nanorods from the ZnO/C/MnO_2 NRAs and ZnO/MnO_2 NRAs in 0.25 M NaOH solution, respectively.

Sample Characterizations. The surface morphologies of the fabricated samples were characterized using an environmental SEM (scanning electron microscope, FEI, Quanta 400) and the transmission electron microscope (TEM, JEM-2010HR). The fabricated samples were also analyzed by XRD (power X-ray diffraction, Bruker, D8). EDS (X-ray energy dispersive spectroscopy), XPS (X-ray photoelectron spectroscopy, ESCA-LAB 250), and laser micro-Raman spectroscopy (Renishaw inVia) were used to study the chemical compositions and structures of the products.

Electrochemical Characterizations of the C/MnO_2 DNTAs and Symmetrical Supercapacitors (SSCs) Composed of C/MnO_2 DNTAs. Electrochemical measurements of the C/MnO_2 DNTAs were performed in a three-electrode electrolytic cell (The specific mass loading is 0.22 mg/cm^2.). A Na_2SO_4 solution (1.0 mol/L) was used as electrolyte. The counter electrode used a Pt foil, and the reference electrode used an Ag/AgCl electrode. Before measurements, the working electrodes of C/MnO_2 DNTAs and MnO_2 NTAs were impregnated with electrolyte to let them thoroughly wet for 30 min. A CHI 660C electrochemical workstation (Shanghai Chenhua Instruments Co.) was utilized to measure the electrochemical properties of samples at room temperature. Cyclic voltammometry was measured in the potential range of 0−0.8 V at 5−100 mV/s. EIS (electrochemical impedance spectroscopy) was also measured to study the conductivity of C/MnO_2 DNTAs in 1.0 M Na_2SO_4 solution in a three-electrode cell. The EIS was measured at an open-circuit potential of 0.32 V over the frequency range of 1−10 kHz by applying an alternating-current perturbation of 10 mV. The symmetrical supercapacitors (SSCs) were built with two identical C/MnO_2 DNTAs electrodes that were separated with a separator. Before assembling, the two electrodes and the separator were impregnated with electrolyte for 30 min to make them thoroughly wet. The cyclic voltammometry and galvanostatic charge-discharge curves were measured by a two-electrode test to determine the electrochemical performance of SSCs.

RESULTS AND DISCUSSION

Scheme 1 shows the procedures utilized to fabricate the C/MnO_2 DNTAs, and they are described in detail in the Experimental Section. ZnO NRAs, ZnO/C NRAs, and ZnO/C/MnO_2 NRAs are sequentially fabricated, and finally the C/MnO_2 DNTAs were synthesized by dissolving ZnO from the ZnO/C/MnO_2 NRAs. Figures 1a and 1b show SEM images of the ZnO NRAs and ZnO/C NRAs, respectively. From Figure 1b-d, it is clearly observed that the carbon shells are uniformly coated on the ZnO NRAs surfaces with thicknesses of about 30−50 nm. XRD of ZnO/C NRAs is shown in Figure 1e(2), which is similar to the XRD of pure ZnO nanorods. Besides the peaks of ZnO nanorods and Ti substrate, no carbon peak is observed. This means the carbon shells are amorphous. Raman spectrum of ZnO/C NRAs shows two peaks at 1368 and 1602 cm^{-1} as shown in Figure 1f, which corresponds to sp^3 and sp^2 peaks of carbon, respectively, indicating the existence of carbon shells.[35] Figure 2a shows SEM image of the ZnO/C/MnO_2 core-shell NRAs, and it shows MnO_2 shells are uniformly coated on the surfaces of ZnO/C NRAs. The typical SEM image of the fabricated C/MnO_2 DNTAs is shown in Figure 2b, which clearly shows that the large-scale and orderly C/MnO_2 DNTAs are successfully fabricated. The diameters and lengths of C/MnO_2 DNTAs are about 650 nm and 3.0 μm, respectively. The hollow nanotube arrays and large open space between the neighboring nanotubes in C/MnO_2 DNTAs will allow facile electrolyte diffusion throughout the film electrode as shown in Figure 2f.

More structure details are examined by TEM, and Figure 2c shows the typical TEM image of C/MnO_2 DNTAs. The thicknesses of carbon and MnO_2 layers are about 35 and 100 nm, respectively The high-resolution transmission electron microscopy (HRTEM) image measured from MnO_2 layer is shown in Figure 2d, and the SAED pattern is present in Figure 2e, which both show the amorphous structures of MnO_2 layers. Figure 2g shows XPS spectrum in the energy region of Mn 2p for C/MnO_2 DNTAs. Two detected peaks at 642.3 eV and 654.1 eV correspond to Mn $2p_{3/2}$ and $2p_{1/2}$, respectively, and this result indicates that the element Mn is present in Mn(IV),[36] which corresponds to MnO_2 in deposits. Figure 2h shows XPS spectrum in the energy region of C 1s for C/MnO_2 DNTAs. The peak at 284.8 eV shows the existence of carbon in products.[37] Based on the above analyses, the C/MnO_2 DNTAs were successfully fabricated. TGA and DTG curves of the C/MnO_2 DNTAs and MnO_2 NTAs are shown in Figure S2, which shows the weight fraction of MnO_2 in the C/MnO_2 DNTAs is about ~98.94 wt %. Figure S3 shows the EDX and XRD results of C/MnO_2 DNTAs. The element of Zn is not seen in Figure S3a. The ZnO peak is not observed in C/MnO_2 double-walled nanotube structures as shown in Figure

Scheme 1. Schematic Illustration for the Synthesis of C/MnO_2 DNTAs

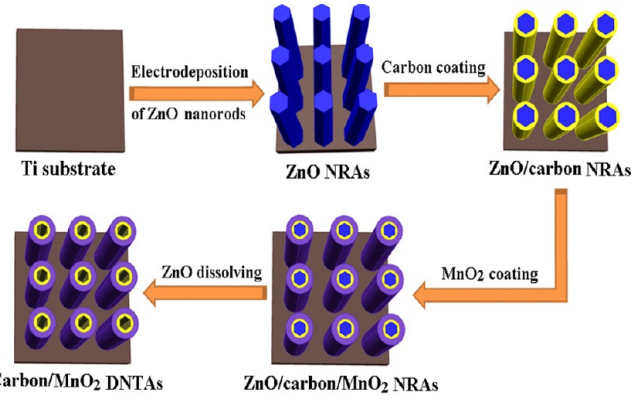

(**NRAs**: nanorod arrays; **DNTAs**: double-walled nanotube arrays)

dx.doi.org/10.1021/am405271q | ACS Appl. Mater. Interfaces 2014, 6, 2726−2733

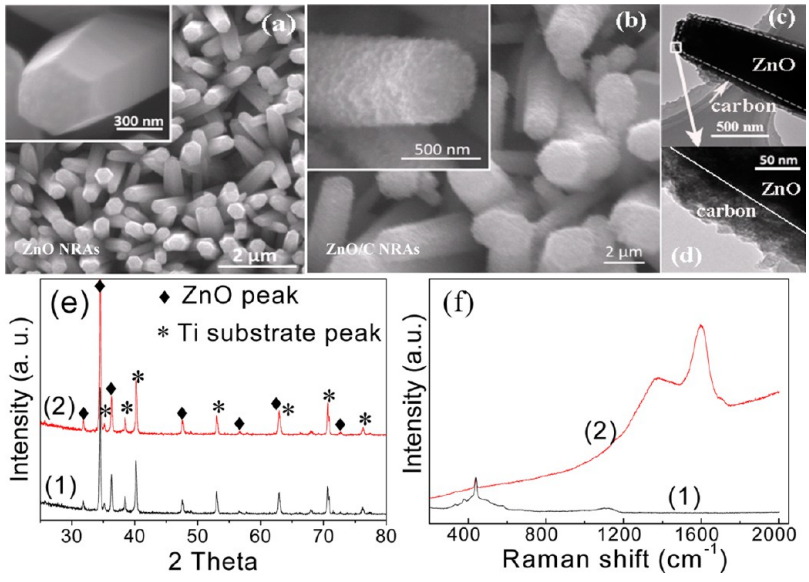

Figure 1. SEM images of (a) ZnO NRAs and (b) ZnO/C NRAs; (c–d) TEM images of a ZnO/C nanorod with different magnifications; (e) XRD and (f) Raman spectra of (1) ZnO NRAs and (2) ZnO/C NRAs.

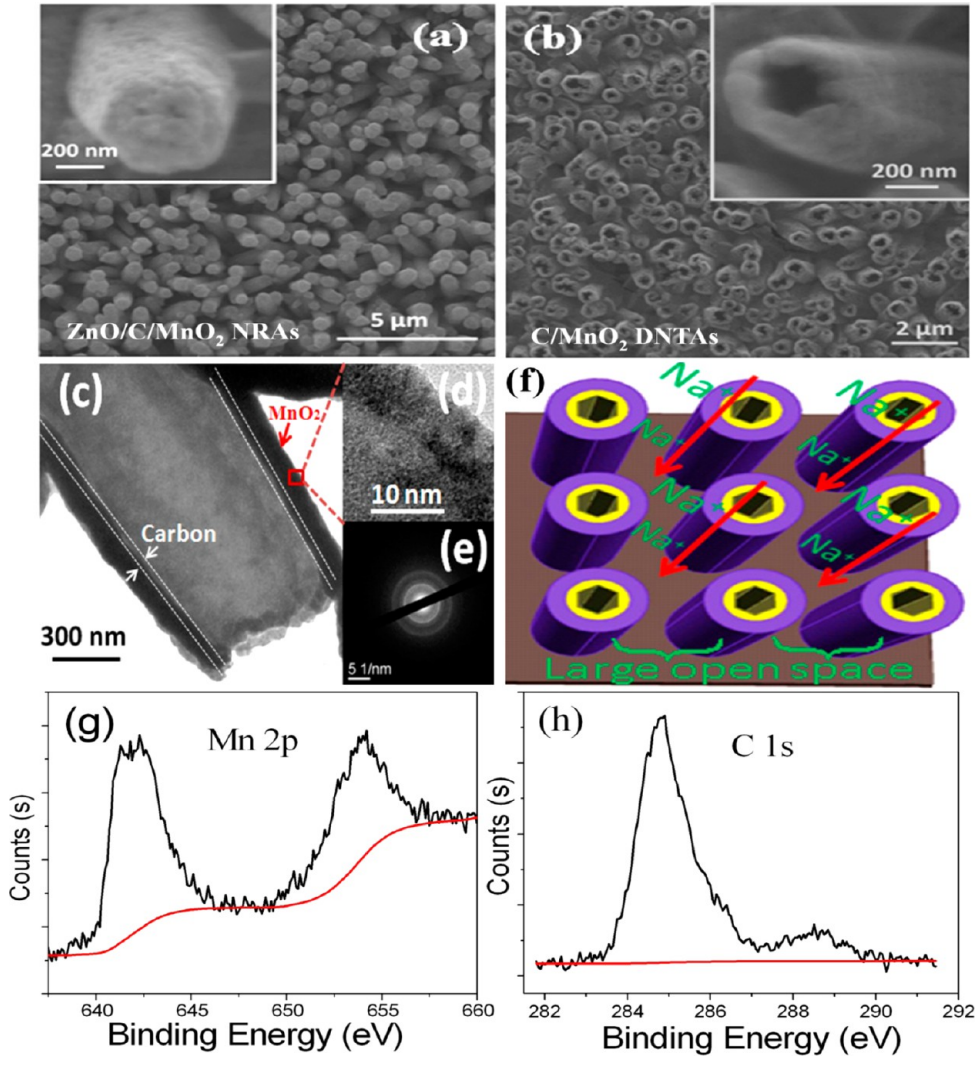

Figure 2. (a) SEM image of ZnO/C/MnO_2 NRAs; (b) SEM image of C/MnO_2 DNTAs; (c-d) TEM images and (e) SAED pattern of C/MnO_2 DNTAs; (f) Schematic illustration for the advantage of C/MnO_2 DNTAs. (g) XPS spectrum of Mn 2p; (h) XPS spectrum of C 1s.

dx.doi.org/10.1021/am405271q | ACS Appl. Mater. Interfaces 2014, 6, 2726–2733

S3b. So the results of EDX and XRD confirm the complete dissolution of ZnO template. The specific surface area of C/MnO_2 DNTAs was obtained by the BET method on the basis of the desorption branch of the nitrogen sorption isotherms that are shown in Figure S4, and the C/MnO_2 DNTAs give a high BET specific surface area of about 55.75 m^2 g^{-1}.

Such design of the hybrid C/MnO_2 DNTAs will allow for maximizing the performance of an electrode because of the geometrical (i.e. DNTA structure) properties and compositional (i.e. multicomponent composites), and the following advantages will be provided: (*i*) The C/MnO_2 DNTAs with anisotropic morphology, hollow nanotube structure, and large surface area will create fast diffusion paths for ions, which will obviously enhance ion transmission and electrode utilization rate as shown in Figure 3a. (*ii*) The weight fraction of

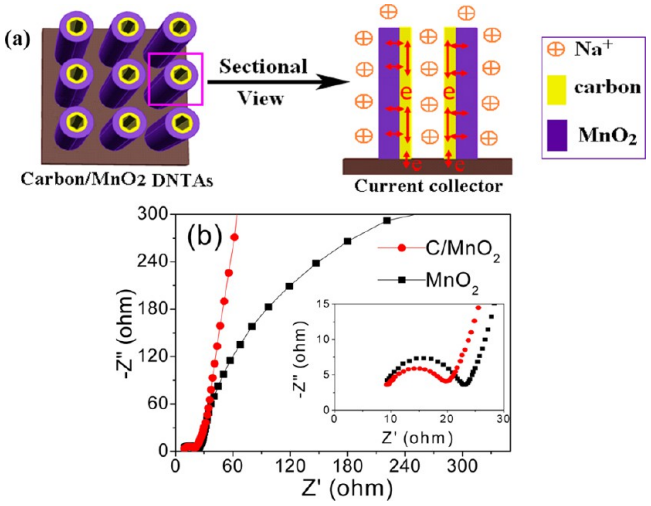

Figure 3. (a) Nanotube array, double-walled nanostructure, and high conductivity in electrode provide fast ion and electron transmission; (b) Nyquist plots for C/MnO_2 DNTAs and MnO_2 NTAs.

supercapacitive MnO_2 in C/MnO_2 DNTAs is high (~98.94%) because the carbon layer is thin and light, so high energy and power densities will be achieved because of the high C_{sp} of C/MnO_2 DNTAs. (*iii*) The conductive networks will be well-built in the electrode since the MnO_2 layers are attached tightly on carbon layers that will provide electron "highways" (~0.33 S/cm) for charge transmission because of the high electrical conductivity of carbon and the C/MnO_2 DNTAs directly grow on the Ti substrate with superior electrical contact as shown in Figure 3a. Here the conductibility of C/MnO_2 DNTAs is studied by EIS measurement. The Nyquist plot of C/MnO_2 DNTAs between 1 Hz and 10 kHz is shown in Figure 3b. The equivalent circuit of Nyquist plots of C/MnO_2 DNTAs is shown in Figure S5, where C_{dl} is a double-layer capacitor, C_L is the limit pseudocapacitor, R_s is the solution resistance, R_w is the Warburg impedance, and R_{ct} is the charge transfer resistance. Based on the results in Figure 3b, the C/MnO_2 DNTAs shows smaller R_{ct}, indicating that the carbon nanolayers can obviously reduce the charge transfer resistance, thus improving the transport and collection of electrons in electrode. The higher conductibility of C/MnO_2 DNTAs than MnO_2 NTAs will favor rate capability for the fast charge-discharge and high power performance. In addition, the high conductibility of C/MnO_2 DNTAs will enhance the utilization rate of the electrode because of the slight polarization.

To explore the performance of C/MnO_2 DNTAs for SCs, cyclic voltammetry measurements were performed in an aqueous solution of 0.5 M Na_2SO_4 by the half-cell test (a three-electrode configuration). Cyclic voltammograms (CVs) of C/MnO_2 DNTAs among 0−0.8 V at sweep rates of 5−50 mV/s are shown in Figure 4a. It is seen that the CVs exhibit rectangular-like shapes, which indicate well supercapacitive behaviors. The C_{sp} of C/MnO_2 DNTAs is obtained to be 793 F/g at current density of 1.5 A/g, which is much higher than 319 F/g of MnO_2 NTAs at the same scan rate (SEM image of MnO_2 NTAs is shown in Figure S6c). Figure 4b shows the dependences of C_{sp} of C/MnO_2 DNTAs and MnO_2 NTAs on scan rates. With the scan rate increasing, the C_{sp} usually shows decay because of ion diffusion limitation in solution.[38] Here the C/MnO_2 DNTAs show C_{sp} decay of about 17.3% with the scan rate increasing from 5 to 50 mV/s. Even at 50 mV/s, the C_{sp} of C/MnO_2 DNTAs still obtain 659 F/g. Nevertheless, compared with C/MnO_2 DNTAs, the MnO_2 NTAs show a serious C_{sp} decay of 41.4% with the scan rate increasing from 5 to 50 mV/s and a small C_{sp} of 178 F/g at 50 mV/s. Therefore, the above results in Figure 4b show the C/MnO_2 DNTAs have a much larger C_{sp} and a much better rate capability than MnO_2 NTAs at various scan rates.

Figure S7a shows galvanostatic charge-discharge curves of the C/MnO_2 DNTAs in the half-cell at different current densities, and a symmetric nature in charging/discharging curves is seen, indicating superior reversible redox reactions and good supercapacitive characteristic. Figure 4c shows the summary plot of C_{sp} vs current density, which also demonstrates the C/MnO_2 DNTAs exhibit significantly enhanced supercapacitive performance comparing with MnO_2 NTAs. With current density increasing from 1.0 to 10 A/g, the C/MnO_2 DNTAs show ~25.5% C_{sp} loss, which is much smaller than ~54.4% C_{sp} loss of MnO_2 NTAs, so this result also demonstrates the C/MnO_2 DNTAs have a much better rate capability than MnO_2 NTAs.

In the half-cell test, the C/MnO_2 DNTAs also show excellent long-term cycle life, which is highly important for practical SC operations. Figure 4d shows the C_{sp} variation of C/MnO_2 DNTAs as a function of cycle number at 5 mV/s, and it shows no any significant decrease in C_{sp} after 5000 cycles. The C_{sp} retention of C/MnO_2 DNTAs still keep ~97%. However, the MnO_2 NTAs only show the C_{sp} retention of ~69% after 5000 cycles, which is much smaller than 97% of C/MnO_2 DNTAs. The above results demonstrate that the C/MnO_2 DNTAs as electrode materials are much higher stability than MnO_2 NTAs.

Herein, the advantages of C/MnO_2 DNTAs as electrodes for SCs were further investigated in the half-cell test. Figure 5 shows cycling performance of the C/MnO_2 DNTAs at progressively increased and decreased current density, and it indicates that the fabricated C/MnO_2 DNTAs still own high cycle stability after the electrode suffered from sudden current density change. Therefore, the synthesized C/MnO_2 DNTAs own both superior rate capability and excellent long-term cycle life, which are very important for the practical utilizations in the supercapacitors.

To show the feasibility of C/MnO_2 DNTAs for SCs, a simple symmetrical supercapacitor (SSC) based on two small pieces of thin films (1.0 cm^2) of C/MnO_2 DNTAs was presented for a demo as shown in Figure 6 (the electrolyte is 1.0 mol/L Na_2SO_4 solution, and it was dripped on the surfaces of thin films). Here we found that this device could power a red light-

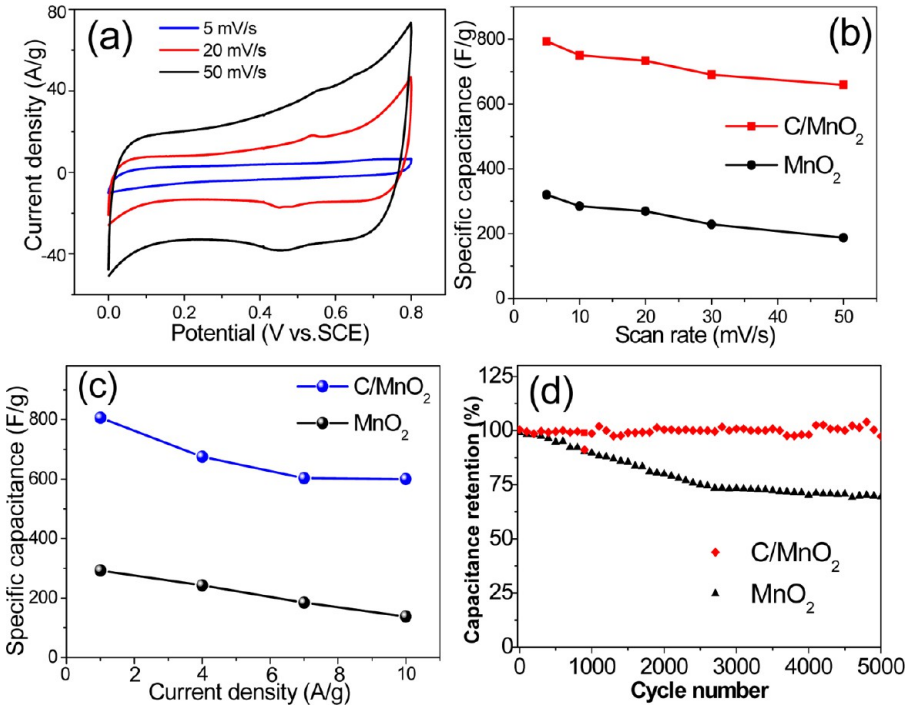

Figure 4. (a) CV curves of a half-cell of C/MnO_2 DNTAs at various scan rates of 5, 20, and 50 mV/s; (b) Summary plots of C_{sp} at various scan rates for the half-cells of C/MnO_2 DNTAs and MnO_2 NTAs; (c) Summary plots of C_{sp} at different current densities for the half-cells of C/MnO_2 DNTAs and MnO_2 NTAs; (d) Cycling performance of the half-cells of C/MnO_2 DNTAs and MnO_2 NTAs for 5000 cycles at current density of 1.5 A/g.

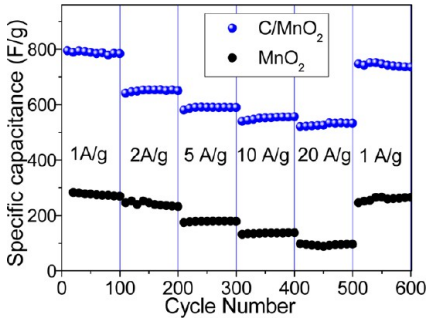

Figure 5. Cycling stability a half-cell of C/MnO_2 DNTAs at progressively varied current densities.

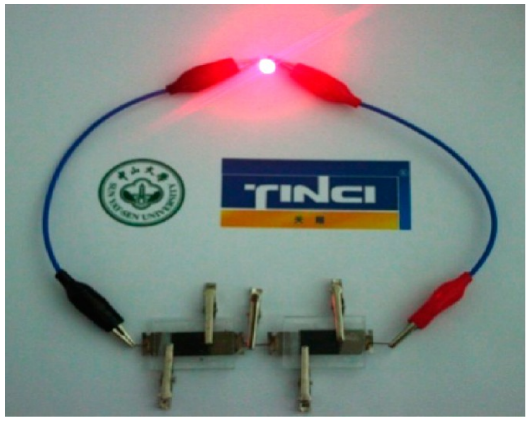

Figure 6. Red light-emitting diode (LED) lighting demonstration, with the diode driven by a simple fabricated supercapacitor.

emitting diode (LED) for about 8 min after charging at 1.0 mA/cm^2 for 30 s.

Cyclic voltammetry measurements of the SSC based on C/MnO_2 DNTAs were performed in 0.5 M Na_2SO_4 solution on a two-electrode test configuration as shown in Figure 7a. The C_{sp} of the SSC of C/MnO_2 DNTAs is obtained to be 161 F/g at 5 mV/s, which is much higher than 66 F/g of the SSC of MnO_2 NTAs at the same sweep rate. The SSC of C/MnO_2 DNTAs shows a C_{sp} decay of about 20.87% with the scan rate increasing from 5 to 100 mV/s as shown in Figure 7b. Even at a scan rate as large as 100 mV/s, the SSC of C/MnO_2 DNTAs still achieves a value as high as 127 F/g. However, compared with the SSC of C/MnO_2 DNTAs, the SSC of MnO_2 NTAs shows a serious C_{sp} decay of 55.73% with the scan rate increasing from 5 to 100 mV/s and a small C_{sp} of 29 F/g at 100 mV/s. Figure S8 shows galvanostatic charge-discharge curves of the SSC of carbon/MnO_2 DNTAs and SSC of MnO_2 NTAs at different current densities. Figure 7c shows the summary plot of C_{sp} vs current density, which demonstrates the SSC of C/MnO_2 DNTAs exhibit significantly enhanced supercapacitive performance comparing with that of MnO_2 NTAs. The SSC of C/MnO_2 DNTAs shows the improved long-term cycle life. The C_{sp} variation as a function of cycle number of the SSC of C/MnO_2 DNTAs at 0.75 A/g is shown in Figure 7d, which shows the SSC of C/MnO_2 DNTAs almost can undergo more than 10,000 cycles without an obvious decrease in C_{sp}. After 10,000 cycles, the C_{sp} retention of SSC of C/MnO_2 DNTAs still keeps ~85%. However, the MnO_2 NTAs only show the C_{sp} retention of ~62% after 10,000 cycles, indicating a much worse cycle stability. The above results demonstrate that the SSC of C/MnO_2 DNTAs is much higher stability than the SSC of MnO_2 NTAs during the long-term cycling test.

Figure 8a shows the cycling performance of the SSC of C/MnO_2 DNTAs on a two-electrode test configuration at progressively increased and decreased current density. The SSC of C/MnO_2 DNTAs still shows high cycle stabilities at

dx.doi.org/10.1021/am405271q | ACS Appl. Mater. Interfaces 2014, 6, 2726−2733

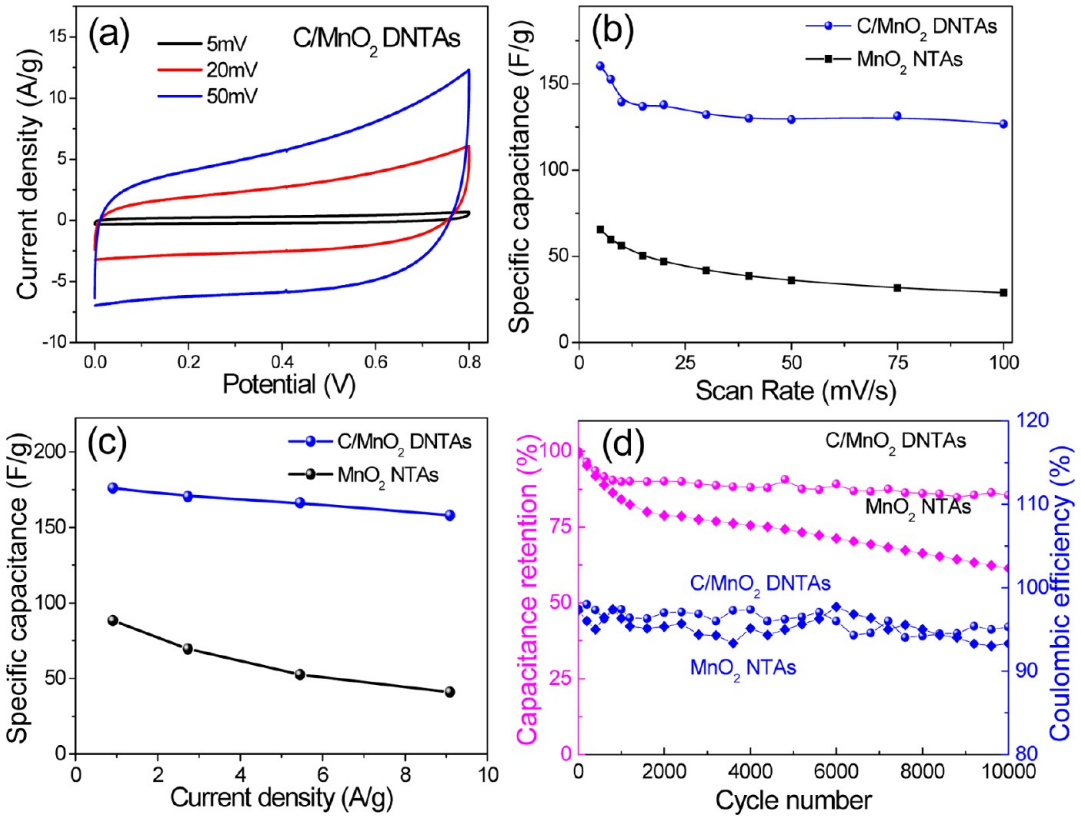

Figure 7. (a) CVs of symmetrical supercapacitor (SSC) based on the C/MnO_2 DNTAs and MnO_2 NTAs at scan rates of 5, 20, and 50 mV/s; (b) Summary plots of C_{sp} at different scan rates for SSCs based on the C/MnO_2 DNTAs and MnO_2 NTAs; (c) Summary plots of C_{sp} at various current densities for SSCs based on the C/MnO_2 DNTAs and MnO_2 NTAs; (d) Cycling performance and coulombic efficiency of SSCs based on the C/MnO_2 DNTAs and MnO_2 NTAs for 10000 cycles at 0.75 A/g.

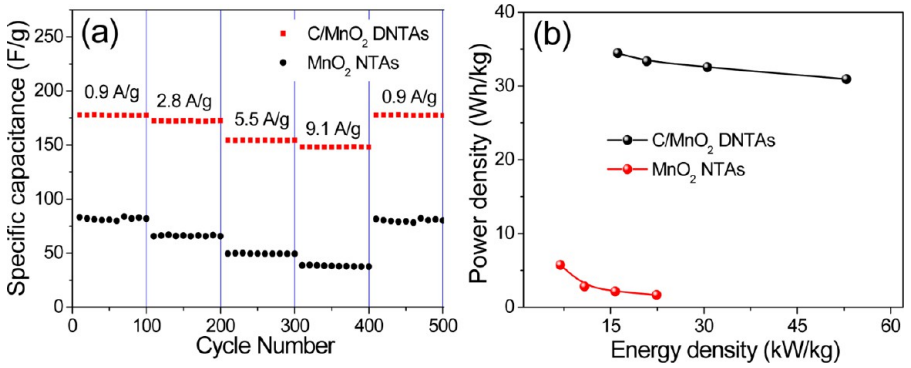

Figure 8. (a) Cycle life at progressively changed current densities of SSCs based on the C/MnO_2 DNTAs and MnO_2 NTAs; (b) Ragone plots of SSCs based on the C/MnO_2 DNTAs and MnO_2 NTAs.

various current densities after the electrode suffered from sudden current density change. The energy and power densities of the SSC of C/MnO_2 DNTAs are also studied because they are highly important for electrochemical devices. Figure 8b shows the Ragone plot, and it inidcates the SSC of C/MnO_2 DNTAs can provide a high energy density of ~40 Wh/kg, much superior to the SSC of MnO_2 NTAs and the conventional SSCs. In addition, the C/MnO_2 DNTAs also can provide the highest power density of 16 KW/kg, which is higher than the power demand of PNGV (Partner-ship for a New Generation of Vehicles), 15 KW/kg, indicating the superior capability of the SSC of C/MnO_2 DNTAs.

The volumetric performance of the SSC of C/MnO_2 DNTAs on a two-electrode test configuration is also investigated, and it is shown in Figure 9. The volumetric C_{sp} of SSC of C/MnO_2 DNTAs at 5 mV/s is calculated to be 177 mF/cm^3, which is much larger than 72 mF/cm^3 of the SSC of MnO_2 NTAs at the same scan rate. The dependence of volumetric C_{sp} of the SSC of C/MnO_2 DNTAs and MnO_2 NTAs on the scan rate is shown in Figure 9a. With the scan rate increasing from 5 to 100 mV/s, the volumetric C_{sp} of the SSC of C/MnO_2 DNTAs shows a decay of about 21.47%. However, compared with C/MnO_2 DNTAs, the SSC of MnO_2 NTAs shows a serious C_{sp} decay of 55.56% with the scan rate increasing from 5 to 100 mV/s and a small volumetric C_{sp} of 32 F/cm^3 at 100 mV/s. With current density increasing from 0.2 to 2.0 mA/cm^2, the SSC of C/MnO_2 DNTAs shows a much larger volumetric C_{sp} than MnO_2 NTAs as shown in Figure 9b, and they only show

dx.doi.org/10.1021/am405271q | ACS Appl. Mater. Interfaces 2014, 6, 2726−2733

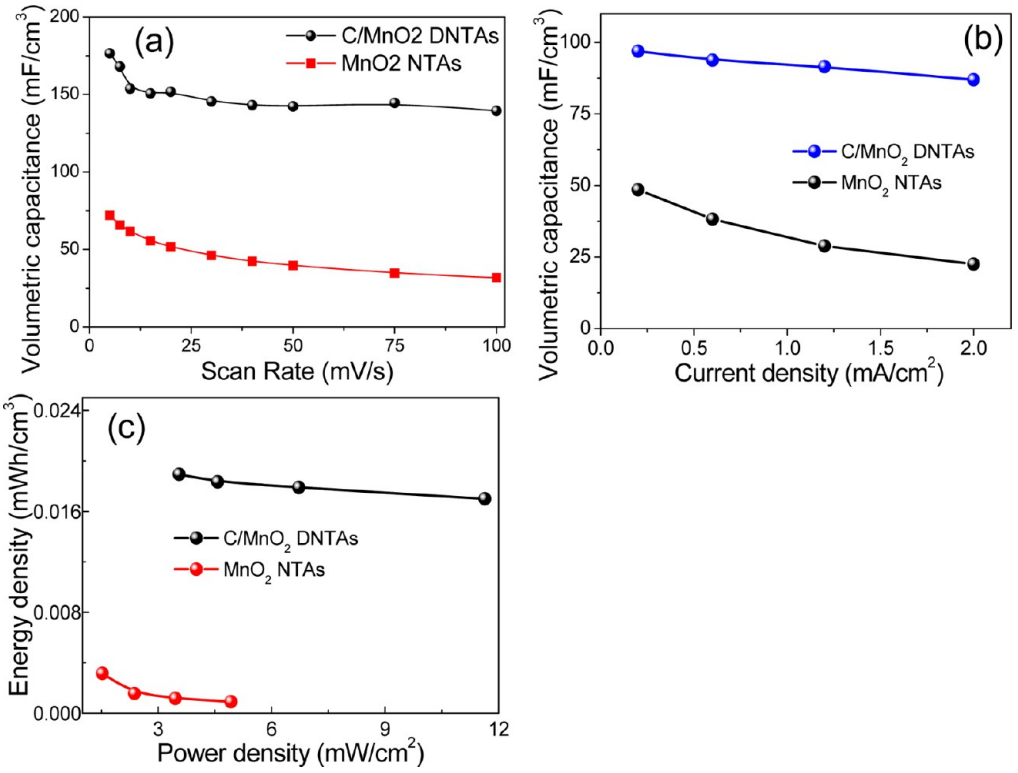

Figure 9. (a) Summary plots of volumetric C_{sp} of the SSCs based on C/MnO_2 DNTAs and MnO_2 NTAs at different scan rates; (b) Summary plots of volumetric C_{sp} of the SSCs based on C/MnO_2DNTAs and MnO_2 NTAs at various current densities; (c) Ragone plots of the SSCs based on C/MnO_2 DNTAs and MnO_2 NTAs.

~10.31% volumetric C_{sp} loss, which is much smaller than ~53.39% C_{sp} loss of MnO_2 NTAs. In addition, the SSC of C/MnO_2 DNTAs shows much larger volumetric power density and energy density than the SSC of MnO_2 NTAs as shown in Figure 9c.

CONCLUSIONS

In conclusion, the novel hybrid C/MnO_2 DNTAs as electrodes were designed for SC applications. The unique DNTA architectures of C/MnO_2 composites permit a high utilization ratio of electrode with the facilitated ion and electron transmission. The designed C/MnO_2 DNTAs show superior supercapacitive performance, such as large C_{sp}, high energy/power densities, and superior long-term cycle life. The hollow nanotube structures, double-walled structures, orderly pore passages, and high conductivity are mainly responsible for the much improved supercapacitive performance of the C/MnO_2 DNTAs. The SSCs composed of C/MnO_2 DNTAs also show the predominant performance, indicating the C/MnO_2 DNTAs are promising materials for SCs. The design and synthesis strategy of electrode materials reported in this study can be used for other metal oxides, such as Co_3O_4, NiO, and V_2O_5, to build carbon-based hybrid DNTAs and other double-walled hollow nanostructures that will be very promising for various electrochemical devices, such as batteries and sensors.

ASSOCIATED CONTENT

Supporting Information

SEM, TG, DTG, EDS, XRD, adsorption-desorption isotherms, and galvanostatic charge-discharge curves. This material is available free of charge via the Internet at http://pubs.acs.org.

AUTHOR INFORMATION

Corresponding Authors

*E-mail: chedhx@mail.sysu.edu.cn.
*E-mail: ligaoren@mail.sysu.edu.cn.

Notes

The authors declare no competing financial interest.

ACKNOWLEDGMENTS

This work was supported by NSFC (51173212 and 21073240), Natural Science Foundation of Guangdong Province (S2013020012833), Fundamental Research Fund for the Central Universities (13lgpy51), Fund of New Star Scientist of Pearl River Science and Technology of Guangzhou (2011J2200057), SRF for ROCS, SEM ([2012]1707), and Open-End Fund of State Key Lab of Physical Chemistry of Solid Surfaces of Xiamen University (201113).

REFERENCES

(1) Brezesinski, T.; Wang, J.; Polleux, J.; Dunn, B.; Tolbert, S. H. *J. Am. Chem. Soc.* **2009**, *131*, 1802−1809.
(2) Wang, X.; Liu, B.; Wang, Q.; Song, W.; Hou, X.; Cheng, Y.; Shen, G. *Adv. Mater.* **2013**, *25*, 1479−1486.
(3) Wei, T.-Y.; Chen, C.-H.; Chien, H.-C.; Lu, S.-Y.; Hu, C.-C. *Adv. Mater.* **2010**, *22*, 347−351.
(4) Chen, J.; Sheng, K.; Luo, P.; Li, C.; Shi, G. *Adv. Mater.* **2012**, *24*, 4569−4573.
(5) Chen, L.; Zhang, X.-D.; Liang, H.-W.; Kong, M.; Guan, Q.; Chen, P.; Wu, Z.; Yu, S.-H. *ACS Nano* **2012**, *6*, 7092−7102.
(6) Chen, Z.; Augustyn, V.; Wen, J.; Zhang, Y.; Shen, M.; Dunn, B.; Lu, Y. *Adv. Mater.* **2011**, *23*, 791−795.
(7) Lu, X.; Wang, G.; Zhai, T.; Yu, M.; Gan, J.; Tong, Y.; Li, Y. *Nano Lett.* **2012**, *12*, 1690−1696.

(8) Nyholm, L.; Nyström, G.; Mihranyan, A.; Strømme, M. *Adv. Mater.* **2011**, *23*, 3751−3769.
(9) Xie, K.; Qin, X.; Wang, X.; Wang, Y.; Tao, H.; Wu, Q.; Yang, L.; Hu, Z. *Adv. Mater.* **2012**, *24*, 347−352.
(10) Guan, C.; Li, X.; Wang, Z.; Cao, X.; Soci, C.; Zhang, H.; Fan, H. J. *Adv. Mater.* **2012**, *24*, 4186−4196.
(11) Yang, L.; Cheng, S.; Ding, Y.; Wang, Z. L.; Liu, M. *Nano Lett.* **2012**, *12*, 321−325.
(12) Lu, Q.; Lattanzi, M.; Chen, Y.; Kou, X.; Li, W.; Fan, X.; Unruh, K.; Chen, J. G.; Xiao, J. Q. *Angew. Chem. Int. Ed.* **2011**, *50*, 6847−6850.
(13) Reddy, A. L. M.; Gowda, S. R.; Shaijumon, M. M.; Ajayan, P. M. *Adv. Mater.* **2012**, *24*, 5045−5064.
(14) Chen, S.; Zhu, J.; Wu, X.; Han, Q.; Wang, X. *ACS Nano* **2010**, *4*, 2822−2830.
(15) Liu, J.; Jiang, J.; Cheng, C.; Li, H.; Zhang, J.; Gong, H.; Fan, H. J. *Adv. Mater.* **2011**, *23*, 2076−2081.
(16) Jiang, J.; Li, Y.; Liu, J.; Huang, X.; Yuan, C.; Lou, X. W. *Adv. Mater.* **2012**, *24*, 5166−5180.
(17) Deng, M.-J.; Chang, J.-K.; Wang, C.-C.; Chen, K.-W.; Lin, C.-M.; Tang, M.-T.; Chen, J.-M.; Lu, K.-T. *Energy Environ. Sci.* **2011**, *4*, 3942−3946.
(18) Sassin, M. B.; Chervin, C. N.; Rolison, D. R.; Long, J. W. *Acc. Chem. Res.* **2012**, *46*, 1062−1074.
(19) Li, Q.; Wang, Z.; Li, G.; Guo, R.; Ding, L.; Tong, Y. *Nano Lett.* **2012**, *12*, 3803−3807.
(20) Liang, Y.; Schwab, M.; Zhi, L.; Mugnaioli, E.; Kolb, U.; Feng, X.; Müllen, K. *J. Am. Chem. Soc.* **2010**, *132*, 15030−15037.
(21) Lee, S.; Kim, J.; Chen, S.; Hammond, P. T.; Shao-Horn, Y. *ACS Nano* **2010**, *4*, 3889−3896.
(22) Tang, Z.; Tang, C.; Gong, H. *Adv. Funct. Mater.* **2012**, *22*, 1272−1278.
(23) Fischer, A.; Pettigrew, K.; Rolison, D. R.; Stroud, R. M.; Long, J. W. *Nano Lett.* **2007**, *7*, 281−286.
(24) Bao, L.; Zang, J.; Li, X. *Nano Lett.* **2011**, *11*, 1215−1220.
(25) Lang, X. Y.; Hirata, A.; Fujita, T.; Chen, M. W. *Nat. Nanotechnol.* **2011**, *6*, 232−236.
(26) Lu, X.; Zhai, T.; Zhang, X.; Shen, Y.; Yuan, L.; Hu, B.; Gong, L.; Chen, J.; Gao, Y.; Zhou, J.; Tong, Y.; Wang, Z. L. *Adv. Mater.* **2012**, *24*, 938.
(27) He, Y.-B.; Li, G.-R.; Wang, Z.-L.; Su, C.-Y.; Tong, Y.-X. *Energy Environ. Sci.* **2011**, *4*, 1288−1292.
(28) Wang, Z.-L.; Guo, R.; Ding, L.-X.; Tong, Y.-X.; Li, G.-R. *Sci. Rep.* **2013**, *3*, 1204.
(29) Liu, R.; Duay, J.; Lee, S. B. *ACS Nano* **2011**, *5*, 5608−5619.
(30) Jiang, H.; Ma, J.; Li, C. *Adv. Mater.* **2012**, *24*, 4197−4202.
(31) Yu, G.; Hu, L.; Vosgueritchian, M.; Wang, H.; Xie, X.; McDonough, J.; Cui, X.; Cui, Y.; Bao, Z. *Nano Lett.* **2011**, *11*, 2905−2911.
(32) Yu, G.; Hu, L.; Liu, N.; Wang, H.; Vosgueritchian, M.; Yang, Y.; Cui, Y.; Bao, Z. *Nano Lett.* **2011**, *11*, 4438−4442.
(33) Kim, J.-H.; Lee, K. H.; Overzet, L. J.; Lee, G. S. *Nano Lett.* **2011**, *11*, 2611−2617.
(34) Hou, Y.; Cheng, Y.; Hobson, T.; Liu, J. *Nano Lett.* **2010**, *10*, 2727−2733.
(35) Zhou, C.; Wang, H.; Peng, F.; Liang, J.; Yu, H.; Yang, J. *Langmuir* **2009**, *25*, 7711−7717.
(36) Koroteev, V.; Bulusheva, L. G.; Asanov, I. P.; Shlyakhova, E. V.; Vyalikh, D. V.; Okotrub, A. V. *J. Phys. Chem. C* **2011**, *115*, 21199−21204.
(37) Li, Q.; Zuo, X.; Liu, J.; Xiao, X.; Shu, D.; Nan, J. *Electrochim. Acta* **2011**, *58*, 330−335.
(38) Zhao, X.; Zhang, L.; Murali, S.; Stoller, M. D.; Zhang, Q.; Zhu, Y.; Ruoff, R. S. *ACS Nano* **2012**, *6*, 5404−5412.